Solutions of the Faddeev-Yakubovsky equations for the four nucleon scattering states

F. Ciesielski and J. Carbonell
Institut des Sciences Nucléaires, 53, Avenue des Martyrs, 38026 Grenoble, France
(Received 12 February 1998)

The Faddeev-Yakubowsky equations in configuration space have been solved for the four nucleon system. The results with an S-wave interaction model in the isospin approximation are presented. They concern the bound and scattering states below the first three-body threshold. The elastic phase shifts for the $N+NNN$ reaction in different (S,T) channels are given and the corresponding low-energy expansions are discussed. Particular attention is paid to the $n+t$ elastic cross section. Its resonant structure is well described in terms of a simple NN interaction. First results concerning the S matrix for the coupled $N+NNN$-$NN+NN$ channels and the strong deuteron-deuteron scattering length are obtained. [S0556-2813(98)04607-X]

PACS number(s): 21.45.+v, 11.80.Jy, 25.40.Hs, 25.10.+s

I. INTRODUCTION

The four nucleon bound state calculations have, in the last years, reached a high level of accuracy and consistency at least as far as the solutions of the corresponding equations are concerned [1–4]. This situation contrasts with the $4N$ scattering problem where despite some pioneering and relevant results [5–14], there is a manifest lack of convergence among the different groups and methods even when using simple interactions. This problem is not only a general extension of the three-body one in the sustained task of the nuclear few-body community to deal with increasingly complex systems, but we believe it constitutes a qualitative jump in our understanding of nuclear systems. Indeed the continuum spectrum of the $4N$ system (see Fig. 1), with its rich variety of thresholds and structures, provides a bridge between the relative simplicity of the $A=2,3$ problems and the complexity of many-body systems. Even when restricted to the energies below the first three-body breakup threshold, the presence of several resonances at each Z channel, the existence of the almost degenerate $p+t$ and $n+{}^3$He thresholds with, in the middle, the first 0^+ excitation of the ^{4}He ground state make the understanding of the $A=4$ chart in terms of fundamental NN interactions an exciting and redoubtable theoretical challenge.

We present here the first solution of the Faddeev-Yakubovsky (FY) equations in configuration space for the four nucleon scattering problem. Although the results concerning the bound states (^{4}He and ^{4}He*) will be discussed in some detail, our main interest lies in the $4N$ continuum spectrum, i.e., the $N+NNN$ elastic scattering and its coupling to the first inelastic $NN+NN$ threshold.

The resolution method is based on the angular momentum expansion of the FY amplitudes and the spline expansion of their radial parts. Orthogonal collocation is used to generate a linear system which is solved by iterative procedures. The scattering observables are extracted from a direct inspection of the FY amplitudes in the asymptotic region, in a natural extension of the methods developed for the three-body case in Ref. [15].

The results presented in this paper have all been obtained by using an S-wave NN interaction model and the isospin symmetry hypothesis. The Coulomb and mass difference effects are thus not included. This choice, guided by methodological reasons, allows a presentation of the formalism and methods in a relatively simple framework. Is is remarkable, however, that such a simple model provides a very good description of low-energy scattering observables even if, as in the $n+t$ case, they are not totally trivial. Some first results including realistic interactions have already been reported elsewhere [16] and will be the subject of subsequent publications.

The paper is organized as follows. In the next section we describe the general formalism and the simplifications arising in the case of four identical particles. This section con-

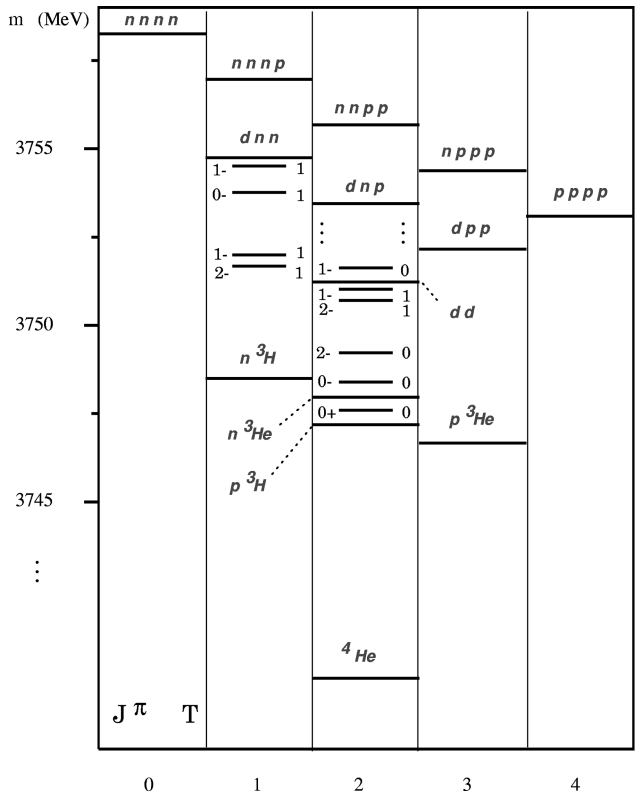

FIG. 1. The $A=4$ chart with the more relevant thresholds and resonances (J^π,T). The vertical axis represents a mass scale; the horizontal one distinguishes the different values of the electric charge Z.

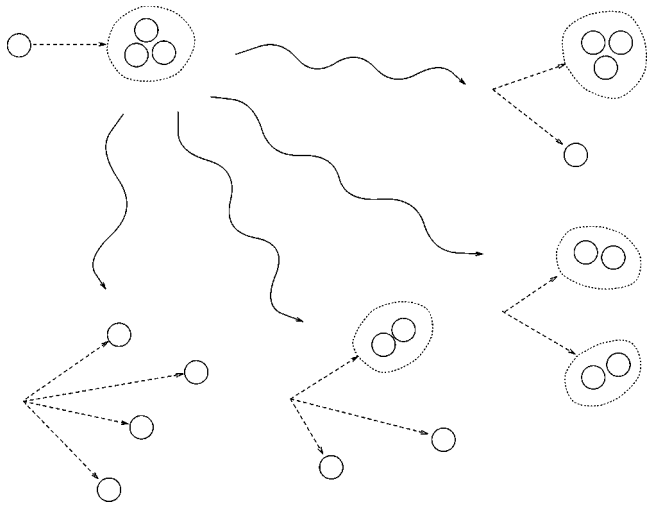

FIG. 2. Different asymptotics to be accounted for in a $1+3$ collision.

tains also the spin, isospin, and angular momentum algebra. In Sec. III we give some details of the numerical methods used. In Sec. IV the results will be presented. They include the ^{4}He ground and first excited state, the elastic phase shifts, and low-energy parameters for the $N+NNN$ reaction and the $N+NNN\rightarrow NN+NN$ first inelastic channel. The energies are restricted below the three- and consequently four-body breakup. Conclusions and perspectives will be given in the last section.

II. THE FORMALISM

A. Faddeev-Yakubovsky equations

With the aim of solving the Schrödinger equation for N particles interacting via a pairwise potential V_{ij}

$$(E-H_0)\Psi=\sum_{i<j} V_{ij}\Psi \tag{1}$$

Yakubovsky [17], generalizing Faddeev's work for $N=3$ [18,19], wrote a set of equations whose solutions verify Eq. (1) and which provides a proper mathematical scheme to account for the variety of physical situations involved (see, e.g., Fig. 2). In the $N=4$ case, the FY equations can be obtained by first splitting the total wave function Ψ in the usual Faddeev amplitudes Ψ_{ij} associated with each interacting pair:

$$\Psi=\sum_{i<j}\Psi_{ij}=\Psi_{12}+\Psi_{13}+\Psi_{14}+\Psi_{23}+\Psi_{24}+\Psi_{34},$$

and requiring them to be a solution of the system of coupled equations

$$(E-H_0)\Psi_{ij}=V_{ij}\sum_{k<l}\Psi_{kl} \tag{2}$$

or equivalently in its integral form

$$\Psi_{ij}=G_0V_{ij}\Psi \tag{3}$$

with

$$G_0=(E-H_0)^{-1}.$$

Each amplitude Ψ_{ij} is in its turn split in three parts, the FY amplitudes, corresponding to the different asymptotics of the remaining two particles:

$$\Psi_{ij}=\Psi^l_{ij,k}+\Psi^k_{ij,l}+\Psi_{ij,kl}, \quad i<j,k<l \tag{4}$$

and obeying the following system of coupled equations:

$$\begin{aligned}
&(E-H_0-V_{ij})\Psi^l_{ij,k}\\
&\quad=V_{ij}(\Psi^l_{ik,j}+\Psi^j_{ik,l}+\Psi_{ik,lj}+\Psi^l_{jk,i}+\Psi^i_{jk,l}+\Psi_{jk,il}),\\
&(E-H_0-V_{ij})\Psi^k_{ij,l}\\
&\quad=V_{ij}(\Psi^k_{il,j}+\Psi^j_{il,k}+\Psi_{il,kj}+\Psi^k_{jl,i}+\Psi^i_{jl,k}+\Psi_{jl,ik}),\\
&(E-H_0-V_{ij})\Psi_{ij,kl}=V_{ij}(\Psi^j_{kl,i}+\Psi^i_{kl,j}+\Psi_{kl,ij}),
\end{aligned} \tag{5}$$

in which an amplitude $\Psi^{\delta}_{\alpha>\beta,\gamma}$, not defined by Eq. (4), has to be understood as being identical to $\Psi^{\delta}_{\beta\alpha,\gamma}$. Any solution of this system of 18 coupled equations, called the FY equations, is a solution of Eq. (2) and consequently of the initial problem (1). Its advantage lies in the possibility to define for system (5) appropriate boundary conditions ensuring the unicity of the solution. Indeed when one of the particles, e.g., labeled by l, is out of reach of the interaction, all the amplitudes in Eq. (5) tend to zero except $\Psi^l_{ij,k}$ and circular permutations on ijk which obey

$$(E-H_0-V_{ij})\Psi^l_{ij,k}=V_{ij}(\Psi^l_{ik,j}+\Psi^l_{jk,i}). \tag{6}$$

This system of equations, resulting from Eq. (5), is equivalent to the $3N$ Faddeev equations for the particles (ijk). In a similar way, when the (ij) and (kl) clusters are free from interaction the only nonvanishing amplitudes are $\Psi_{ij,kl}$ and $\Psi_{kl,ij}$ and their corresponding equations in Eq. (5) tends to

$$(E-H_0-V_{ij})\Psi_{ij,kl}=V_{ij}\Psi_{kl,ij}. \tag{7}$$

It is worth noticing that the FY amplitudes can be written in terms of the Faddeev amplitudes in the form

$$\begin{aligned}
\Psi^l_{ij,k}&=G_{ij}V_{ij}(\Psi_{ik}+\Psi_{jk}),\\
\Psi_{ij,kl}&=G_{ij}V_{ij}\Psi_{kl},
\end{aligned} \tag{8}$$

where

$$G_{ij}=(E-H_0-V_{ij})^{-1}$$

and, according to Eq. (3), in terms of the total wave function

$$\begin{aligned}
\Psi^l_{ij,k}&=G_{ij}V_{ij}G_0(V_{ik}+V_{jk})\Psi,\\
\Psi_{ij,kl}&=G_{ij}V_{ij}G_0V_{kl}\Psi.
\end{aligned} \tag{9}$$

Disregarding the internal degrees of freedom (such as spin, isospin), the natural basis for the configuration space is provided by the positions of the different particles

$$|\vec{r}_1\vec{r}_2\vec{r}_3\vec{r}_4\rangle=|\vec{r}_1\rangle\otimes|\vec{r}_2\rangle\otimes|\vec{r}_3\rangle\otimes|\vec{r}_4\rangle. \tag{10}$$

In order to remove the center of mass motion, it is useful to introduce the relative Jacobi coordinates. Two sets of Jacobi coordinates can be defined for each of the 4! arrangements $(ijkl)$. One of K type,

$$\vec{x}_K(ijkl)=\sqrt{\frac{2\mu_{i,j}}{m}}\,(\vec{r}_j-\vec{r}_i),$$

$$\vec{y}_K(ijkl)=\sqrt{\frac{2\mu_{ij,k}}{m}}\left(\vec{r}_k-\frac{m_i\vec{r}_i+m_j\vec{r}_j}{m_i+m_j}\right),$$

$$\vec{z}_K(ijkl)=\sqrt{\frac{2\mu_{ijk,l}}{m}}\left(\vec{r}_l-\frac{m_i\vec{r}_i+m_j\vec{r}_j+m_k\vec{r}_k}{m_i+m_j+m_k}\right), \tag{11}$$

and one of H type,

$$\vec{x}_H(ijkl)=\sqrt{\frac{2\mu_{i,j}}{m}}\,(\vec{r}_j-\vec{r}_i),$$

$$\vec{y}_H(ijkl)=\sqrt{\frac{2\mu_{k,l}}{m}}\,(\vec{r}_l-\vec{r}_k),$$

$$\vec{z}_H(ijkl)=\sqrt{\frac{2\mu_{ij,kl}}{m}}\left(\frac{m_k\vec{r}_k+m_l\vec{r}_l}{m_k+m_l}-\frac{m_i\vec{r}_i+m_j\vec{r}_j}{m_i+m_j}\right), \tag{12}$$

in which m is an arbitrary mass taken as a reference and $\mu_{\alpha,\beta}$ is the reduced mass of clusters α and β. However, some of these 48 coordinate sets are redundant. For instance those obtained by exchanging $i\leftrightarrow j$ in a K set or $i\leftrightarrow j$ or/and $k\leftrightarrow l$ in the H set are equivalent. This yields 18 $(12K+6H)$ arbitrary and physically nonequivalent Jacobi sets, as many as FY amplitudes. Any of these coordinate sets, suitably completed with the center of mass coordinate $\vec{R}$, constitutes an equivalent description of the four particles configuration space. That provides 18 coordinate sets and the corresponding bases for the configuration space, equivalent to Eq. (10), that will be written in the form $|\vec{x}_K\vec{y}_K\vec{z}_K(ijkl)\vec{R}\rangle$ or $|\vec{x}_H\vec{y}_H\vec{z}_K(ijkl)\vec{R}\rangle$. The degrees of freedom related to the center of mass motion separate in nonrelativistic dynamics and will be hereafter omitted. Although each FY amplitude could be in principle expressed in terms of any of these bases, only one of them is appropriate for expanding it. We will denote the resulting components by

$$\Phi^l_{ij,k}(\vec{x},\vec{y},\vec{z})\equiv\langle\vec{x}_K\vec{y}_K\vec{z}_K(ijkl)|\Phi^l_{ij,k}\rangle,$$

$$\Phi_{ij,kl}(\vec{x},\vec{y},\vec{x})\equiv\langle\vec{x}_H\vec{y}_H\vec{z}_H(ijkl)|\Phi_{ij,kl}\rangle.$$

The bases described above have to be completed to account for other degrees of freedom such as spin, isospin, etc. Further details about the formalism and the relation between the different bases sets can be found, e.g., in Ref. [20].

B. Identical particles

In the case of four identical particles, the 18 FY amplitudes can be obtained by the action of the transposition permutation operators P_{ij} on two of them, arbitrarily chosen provided that one is of K type and the other one of H type. We have taken $K\equiv\Psi^4_{12,3}$ and $H\equiv\Psi_{12,34}$. The four-body problem is solved by determining the two K,H amplitudes which satisfy the following equations:

$$(E-H_0-V)K=V[(P_{23}+P_{13})(\varepsilon+P_{34})K+\varepsilon(P_{23}+P_{13})H], \tag{13}$$

$$(E-H_0-V)H=V[(P_{13}P_{24}+P_{14}P_{23})K+P_{13}P_{24}H], \tag{14}$$

where $\varepsilon=\pm1$ depending on whether the particles are bosons or fermions. The asymptotic equations, i.e., the equivalent of Eqs. (6), (7) are in this case

$$(E-H_0-V)K=\varepsilon V(P_{23}+P_{13})K, \tag{15}$$

$$(E-H_0-V)H=VP_{13}P_{24}H. \tag{16}$$

The total wave function is then given by

$$\Psi=\Psi_{1+3}+\Psi_{2+2},$$

$$\Psi_{1+3}=[1+\varepsilon(P_{13}+P_{23})][1+\varepsilon(P_{14}+P_{24}+P_{34})]K, \tag{17}$$

$$\Psi_{2+2}=[1+\varepsilon(P_{13}+P_{23}+P_{14}+P_{24})+P_{13}P_{24}]H. \tag{18}$$

Each amplitude $\Phi=K,H$ is considered as a function of its natural set of Jacobi coordinates $\vec{x}_\Phi,\vec{y}_\Phi,\vec{z}_\Phi$, defined, respectively, by Eqs. (11) and (12) with $(ijkl)=(1234)$ and $m=m_i$:

$$\vec{x}_K=\vec{r}_2-\vec{r}_1,$$

$$\vec{y}_K=\sqrt{\frac{4}{3}}\left(\vec{r}_3-\frac{\vec{r}_1+\vec{r}_2}{2}\right),$$

$$\vec{z}_K=\sqrt{\frac{3}{2}}\left(\vec{r}_4-\frac{\vec{r}_1+\vec{r}_2+\vec{r}_3}{3}\right),$$

$$\vec{x}_H=\vec{r}_2-\vec{r}_1,$$

$$\vec{y}_H=\vec{r}_4-\vec{r}_3,$$

$$\vec{z}_H=\sqrt{2}\left(\frac{\vec{r}_3+\vec{r}_4}{2}-\frac{\vec{r}_1+\vec{r}_2}{2}\right).$$

They are expanded in angular momentum variables for each coordinate according to

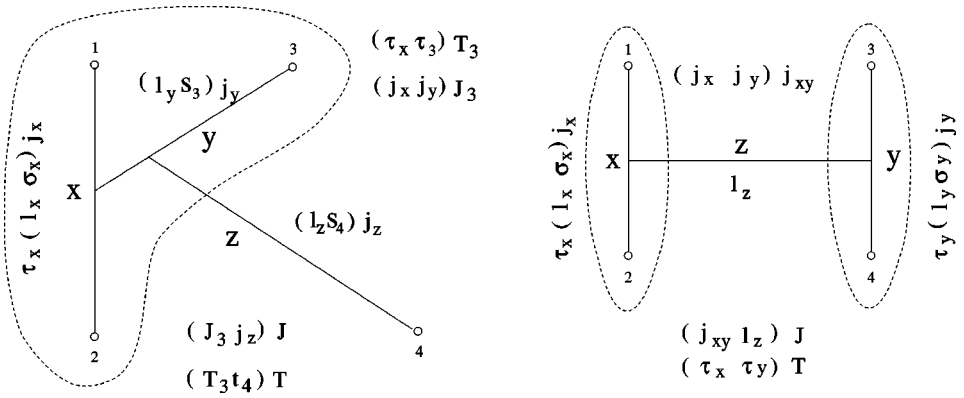

FIG. 3. Spin, isospin, and angular momentum coupling schemes used for the K and H Faddeev-Yakubovsky amplitudes.

$$\langle \vec{x}\vec{y}\vec{z}|\Phi\rangle=\sum_{\alpha}\int\int\int d\hat{x}d\hat{y}d\hat{z}\,\frac{\phi_\alpha(x,y,z)}{xyz}Y_\alpha(\hat{x},\hat{y},\hat{z}), \tag{19}$$

where Y_α are generalized tripolar harmonics containing spin, isospin, and angular momentum variables and the functions ϕ_α, the reduced radial FY components, are the unknowns. The label α represents the set of intermediate quantum numbers defined in a given coupling scheme and includes the specification for the type of amplitudes (K or H). We have used the following couplings, represented in Fig. 3:

K amplitudes:

$$\{[(t_1t_2)_{\tau_x}t_3]_{T_3}t_4\}_T\otimes(\{[l_x(s_1s_2)_{\sigma_x}]_{j_x}(l_ys_3)_{j_y}\}_{J_3}(l_zs_4)_{j_z})_{J^\pi},$$

H amplitudes:

$$[(t_1t_2)_{\tau_x}(t_3t_4)_{\tau_y}]_T\otimes(\{[l_x(s_1s_2)_{\sigma_x}]_{j_x}[l_y(s_3s_4)_{\sigma_y}]_{j_y}\}_{j_{xy}}l_z)_{J^\pi}, \tag{20}$$

where s_i and t_i are the spin and isospin of the individual particles and (J^π,T) are, respectively, the total angular momentum, parity, and isospin of the four-body system. Each component ϕ_α is thus labeled by a set of 12 quantum numbers to which the symmetry properties of the wave function impose the additional constraints: $(-1)^{\sigma_x+\tau_x+l_x}=\varepsilon$ for K and $(-1)^{\sigma_x+\tau_x+l_x}=(-1)^{\sigma_y+\tau_y+l_y}=\varepsilon$ for H. The total parity π is given by $(-)^{l_x+l_y+l_z}$ in both coupling schemes.

The radial equations for the components ϕ_α are obtained by projecting each of Eqs. (13), (14) in its natural configuration space basis $|\vec{x}_\Phi,\vec{y}_\Phi,\vec{z}_\Phi\rangle$. Several steps further [20] we end with a system of coupled integrodifferential equations which, most generally, can be written in the form

$$\sum_{\alpha'}\hat{D}_{\alpha\alpha'}\phi_{\alpha'}(x,y,z)=\sum_{\alpha'}V_{\alpha\alpha'}(x)\sum_{\alpha''}\Bigg[f_{\alpha'\alpha''}\phi_{\alpha''}(x^f_{\alpha'\alpha''},y^f_{\alpha'\alpha''},z^f_{\alpha'\alpha''})+\int_{-1}^{+1}du\,h_{\alpha'\alpha''}(x,y,z,u)\,\phi_{\alpha''}(x^h_{\alpha'\alpha''},y^h_{\alpha'\alpha''},z^h_{\alpha'\alpha''})+\int_{-1}^{+1}du\int_{-1}^{+1}dv\,g_{\alpha'\alpha''}(x,y,z,u,v)\,\phi_{\alpha''}(x^g_{\alpha'\alpha''},y^g_{\alpha'\alpha''},z^g_{\alpha'\alpha''})\Bigg] \tag{21}$$

with

$$\hat{D}_{\alpha\alpha'}=\left(E+\frac{\hbar^2}{m}\Delta_\alpha\right)\delta_{\alpha\alpha'}-V_{\alpha\alpha'}(x),$$

$$\Delta_\alpha=\partial_x^2-\frac{l_x(l_x+1)}{x^2}+\partial_y^2-\frac{l_y(l_y+1)}{y^2}+\partial_z^2-\frac{l_z(l_z+1)}{z^2}.$$

The functions $f_{\alpha'\alpha''},h_{\alpha'\alpha''},g_{\alpha'\alpha''}$ contain all the spin, isospin, and angular momentum couplings. The arguments $x^f_{\alpha'\alpha''},x^h_{\alpha'\alpha''},x^g_{\alpha'\alpha''},\ldots$, are functions of (x,y,z,u,v) in the more general case, and are detailed in the Appendix. The system of equations (21) has been explicitly written in Ref. [21] for the case of four identical bosons.

The FY components for the different (S,T) channels in the S-wave approximation, i.e., with all orbital angular momenta in expansion (19) equal to 0, are listed in Table I. In this table, the symbols $\rightarrow$ and $\sim$ denote, respectively, the amplitudes corresponding to an asymptotic $N+NNN$ or $NN+NN$ channel.

Note that, contrary to the $3N$ problem, the number of FY components appearing in Eq. (21) is infinite even when the pair interaction is restricted to a finite number of partial waves. This divergence comes only from the existence of the l_z additional degree of freedom in the K-like amplitudes.

C. Boundary conditions

For all the physical problems we have considered, the boundary conditions can be written in the Dirichlet form.

TABLE I. Faddeev-Yakubovsky components for (S,T) $4N$ states in the S-wave approximation. The listed quantum numbers are those defined by the coupling schemes (20). The symbols $\rightarrow$ and $\sim$ emphasize, respectively, the asymptotic $N+NNN$ and $NN+NN$ channels.

$S=0$ $(J^\pi=0^+)$ $T=0$

K	τ_x	T_3	l_x	σ_x	j_x	l_y	j_y	$J_3^{\pi_3}$	l_z	j_z
$\rightarrow$	1	1/2	0	0	0	0	1/2	$1/2^+$	0	1/2
$\rightarrow$	0	1/2	0	1	1	0	1/2	$1/2^+$	0	1/2
H	τ_x	τ_y	l_x	σ_x	$j_x^{\pi_x}$	l_y	σ_y	$j_y^{\pi_y}$	j_{xy}	l_z
	1	1	0	0	0^+	0	0	0^+	0	0
$\sim$	0	0	0	1	1^+	0	1	1^+	0	0

$S=1$ $(J^\pi=1^+)$ $T=0$

K	τ_x	T_3	l_x	σ_x	j_x	l_y	j_y	$J_3^{\pi_3}$	l_z	j_z
$\rightarrow$	1	1/2	0	0	0	0	1/2	$1/2^+$	0	1/2
$\rightarrow$	0	1/2	0	1	1	0	1/2	$1/2^+$	0	1/2
	0	1/2	0	1	1	0	1/2	$3/2^+$	0	1/2
H	τ_x	τ_y	l_x	σ_x	$j_x^{\pi_x}$	l_y	σ_y	$j_y^{\pi_y}$	j_{xy}	l_z
	0	0	0	1	1^+	0	1	1^+	1	0

$S=0$ $(J^\pi=0^+)$ $T=1$

K	τ_x	T_3	l_x	σ_x	j_x	l_y	j_y	$J_3^{\pi_3}$	l_z	j_z
$\rightarrow$	1	1/2	0	0	0	0	1/2	$1/2^+$	0	1/2
$\rightarrow$	0	1/2	0	1	1	0	1/2	$1/2^+$	0	1/2
	1	3/2	0	0	0	0	1/2	$1/2^+$	0	1/2
H	τ_x	τ_y	l_x	σ_x	$j_x^{\pi_x}$	l_y	σ_y	$j_y^{\pi_y}$	j_{xy}	l_z
	1	1	0	0	0^+	0	0	0^+	0	0

$S=1$ $(J^\pi=1^+)$ $T=1$

K	τ_x	T_3	l_x	σ_x	j_x	l_y	j_y	$J_3^{\pi_3}$	l_z	j_z
$\rightarrow$	1	1/2	0	0	0	0	1/2	$1/2^+$	0	1/2
$\rightarrow$	0	1/2	0	1	1	0	1/2	$1/2^+$	0	1/2
	1	3/2	0	0	0	0	1/2	$1/2^+$	0	1/2
	0	1/2	0	1	1	0	1/2	$3/2^+$	0	1/2
H	τ_x	τ_y	l_x	σ_x	$j_x^{\pi_x}$	l_y	σ_y	$j_y^{\pi_y}$	j_{xy}	l_z
	1	0	0	0	0^+	0	1	1^+	1	0
	0	1	0	1	1^+	0	0	0^+	1	0

The use of reduced radial FY components ϕ_α in Eq. (19) imposes for any kind of solution the regularity conditions

$$\phi_\alpha(x,y,0)=\phi_\alpha(x,0,z)=\phi_\alpha(0,y,z)=0. \tag{22}$$

For the bound state problem these conditions are completed by forcing the components ϕ_α to vanish on the hypercube $[0,x_N]\times[0,y_N]\times[0,z_N]$, i.e.,

$$\phi_\alpha(x,y,0)=\phi_\alpha(x,y,z_N)=\phi_\alpha(x,0,z)=\phi_\alpha(x,y_N,z)$$
$$=\phi_\alpha(0,y,z)=\phi_\alpha(x_N,y,z)=0. \tag{23}$$

For the scattering problems the boundary conditions are implemented by imposing at large enough values of z the asymptotic behavior of the solutions. Thus, for the $N+NNN$ elastic case we impose at z_N the solution of the $3N$ problem for all the quantum numbers α_a corresponding to the open asymptotic channel a

$$\phi_{\alpha_a}(x,y,z_N)=t_{\alpha_a}(x,y), \tag{24}$$

where the functions $t_{\alpha_a}(x,y)$ are the Faddeev amplitudes of the $3N$ problem. Indeed, at large values of z and for energies below the first inelastic threshold, the solution of Eq. (15) factorizes into a bound state solution of the $3N$ Faddeev equations and a plane wave in the z direction with momentum k_a, whereas the solution of Eq. (16) vanishes. One then has, e.g., for an S wave,

$$\phi_{\alpha_a}(x,y,z)\sim t_{\alpha_a}(x,y)\sin(k_a z+\delta_a) \tag{25}$$

and the scattering observables are directly extracted from the logarithmic derivative of the K amplitude in the asymptotic region:

$$k_a\ \cot(k_a z+\delta_a)=\frac{1}{\phi_{\alpha_a}(x,y,z)}\partial_z\phi_{\alpha_a}(x,y,z). \tag{26}$$

Provided we are in the asymptotic domain, the phase shifts thus extracted have to be independent of (x,y,z) and of the amplitude index α_a. This provides a strong numerical test. An additional advantage of this procedure is that it avoids any cumbersome multidimensional integrals.

In the presence of several open channels, such as $N+NNN$ and $NN+NN$, e.g., several resolutions are needed. The boundary conditions (24) are simply generalized in the form

$$\phi_{\alpha_a}(x,y,z_N)=\lambda_a f_{\alpha_a}(x,y) \tag{27}$$

in which λ_a are arbitrary real numbers and the functions f_{α_a} coincide with t_{α_a} if a is a $N+NNN$ channel or are analogous to the Faddeev amplitudes for Eq. (16) if a is a $NN+NN$ channel.

Equation (24) is generalized in the following way:

$$\varphi_{\alpha_a}(x,y,z)=\Bigg(-\tau_a\hat{h}^-(k_a z)$$
$$+\sum_{a'}\ \tau_{a'}\sqrt{\frac{n_{a'}k_{a'}}{n_a k_a}}\,S_{aa'}\hat{h}^+(k_a z)\Bigg)f_{\alpha_a}(x,y), \tag{28}$$

where $\hat{h}^\pm$ are the regularized Hankel functions [22], and n_a is a multiplicity number for the channel a ($n_a=4$ for $1+3$ and $n_a=3$ for $2+2$ channels) due to the symmetry properties of the total wave function (see, e.g., Ref. [23]). The coefficients τ (amplitudes of the incoming waves) and the S-matrix elements are the unknowns. They are obtained by identifying with the asymptotic form (28) the values $\phi_{\alpha_a},\partial_z\phi_{\alpha_a}$ at z_N for different solutions corresponding to different choices of λ's whose number equals the number of channels. We remark that the momenta k_a appearing in Eqs. (25), (26), (28) are the conjugate variables of the z-Jacobi

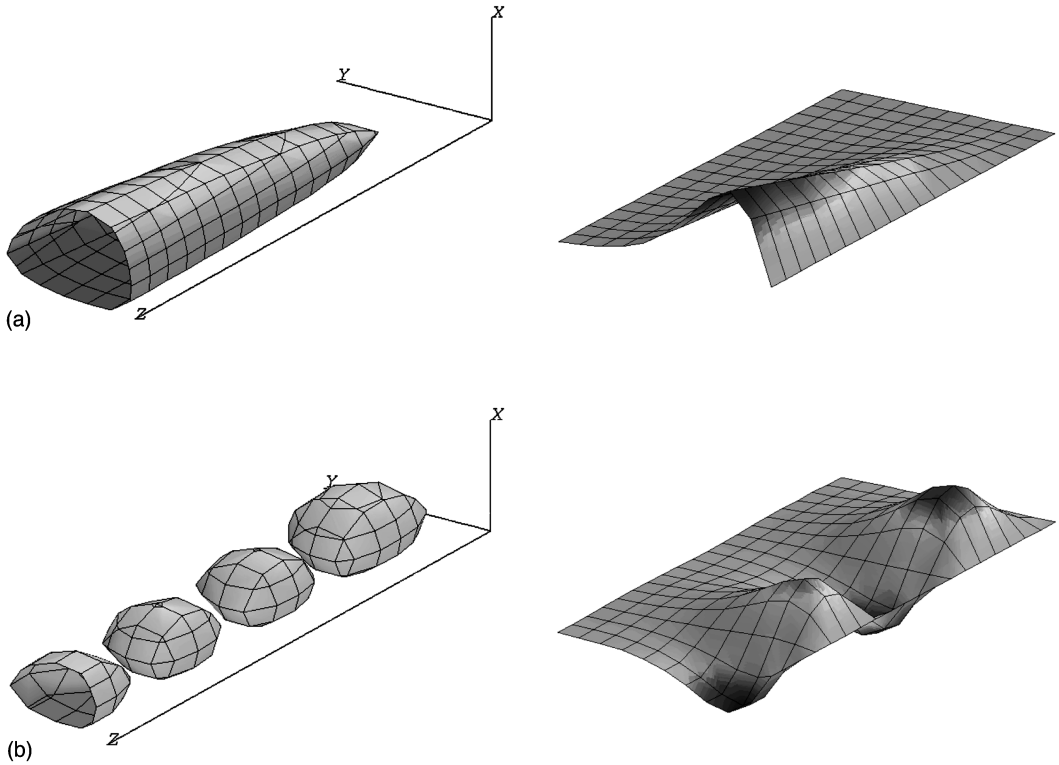

FIG. 4. Representations of some asymptotically nonvanishing amplitudes for $n+t$ elastic scattering: (a) zero-energy, (b) positive kinetic energy. On left, isosurfaces; on right, sections in x variable. The asymptotic factorization between an independent pattern on the x,y coordinates and the z-variable motion appears clearly.

coordinates. They are related to the center of mass kinetic energy E_a of channel a according to $E_a=\hbar^2k_a^2/m$. The physical momenta, conjugate to the physical intercluster distances, are $q_a=\sqrt{\frac{3}{2}}k_a$ or $q_a=\sqrt{2}k_a$ depending whether a corresponds to a $1+3$ or $2+2$ channel.

By the definition (28) one has unitarity ($SS^{\dagger}=1$) and symmetry ($S_{ij}=S_{ji}$) relations. Working with real solutions these properties are related (unitarity implies symmetry). However, none of them is a trivial consequence of the method used but a strong test of numerical accuracy.

In order that the factorizability takes place the asymptotic $3N$ or $2N+2N$ states have to be calculated with the same numerical scheme as that used to solve the four-body problem. This means in practice that they are exact solutions of Eqs. (15) or (16), once the z dynamics are removed. By doing so, the factorization property, valid only in Cartesian coordinates, is an exact numerical property and leads to stable local results. This behavior is illustrated in Fig. 4 in which the FY amplitudes for an $N+NNN$ elastic scattering at $q=0$ and $q>0$ are represented.

III. NUMERICAL METHODS

The numerical methods used are based on the Hermite spline expansion, orthogonal collocation [24], and iterative procedures for solving the linear system. An important step in their solution is the tensor trick [1,25–27].

We look for the solutions ϕ_α of the integrodifferential system (21) in the form of a tensor product of one-dimensional cubic Hermite splines S_i:

$$\phi_\alpha(x,y,z)=\sum_{i=0}^{2N_x+1}\sum_{j=0}^{2N_y+1}\sum_{k=0}^{2N_z+1} c_{\alpha ijk}S_i(x)S_j(y)S_k(z) \tag{29}$$

defined on grids of nonequidistant N_q+1 points $G_q=\{q_0,q_1,\ldots,q_N\}$ where $q\equiv x,y,z$. A grid G_q will be defined by giving the number of intervals N_q, the end point q_N, and the constant scaling factor between two consecutive intervals A_q. We will use the following notation $G\equiv\{N_q,A_q,q_N\}$, often extended to multidomain grids according to $G\equiv\{N_{q1},A_{q1},q_{N1};N_{q2},A_{q2},q_{N2};\cdots\}$.

The boundary conditions are easily implemented using the properties of the spline functions (value and derivative equal to 0 or 1 at the grid points). They result in fixing the values of some of the unknown coefficients $c_{\alpha ijk}$ in the expansion (29). By exchanging the indices of the two last spline functions in each variable the solution takes the form

$$\phi_\alpha(x,y,z)=\sum_{i=1}^{2N_x}\sum_{j=1}^{2N_y}\sum_{k=1}^{2N_z} c_{\alpha ijk}S_i(x)S_j(y)S_k(z) + \sum_{i=1}^{2N_x}\sum_{j=1}^{2N_y} f_{\alpha ij}S_i(x)S_j(y)S_{2N_z+1}(z), \tag{30}$$

where $f_{\alpha ij}$ are the coefficients of the asymptotic functions $f_\alpha(x,y)$ defined in Eq. (27). In the cases of a closed channel or a bound state these coefficients are zero.

Collocation points associated with the three-dimensional grid are used to generate a linear system, the $c_{\alpha ijk}$ being the unknowns. The integral terms in Eq. (21) are calculated with

a Gaussian quadrature rule with typically $N_u, N_v = 6-12$ points in each angular variable u and v. In order to limit the number of parameters we have chosen $N_u = N_v = N_g$.

The number of unknowns is given by $N = 8 N_x N_y N_z N_c$, where $N_c = N_K + N_H$ is the number of FY components. A rough estimation for the extreme cases of a four bosons bound state and of a scattering state in a realistic problem leads to values $N_c = 2-100$, $N_x, N_y = 20-30$, $N_z = 20-40$, and consequently to a number of unknowns going from $N \sim 10^4$ to $N \sim 10^6$. This implies the use of a dense matrix with $\sim 10^{12}$ coefficients. Direct methods are not appropriate for solving such huge linear systems, and we have used iterative techniques, which avoid any storage or inversion of the matrix. The basic feature of any iterative method is to obtain the solution of the linear system only by iterative application of the matrix to an initial vector. This implies a complete calculation of the matrix elements each time it is necessary, and requires the intensive use of parallel computers.

In the case of scattering states, the boundary conditions (27), responsible for the second term in Eq. (30), generate a source term in Eq. (21) leading to a regular linear system of the type $D(E)\vec{c} = [F+G+H]\vec{c} + \vec{b}$, where the different D, F, G, H matrices are reminiscent of the $D_{\alpha\alpha'}, f_{\alpha\alpha'}, g_{\alpha\alpha'}, h_{\alpha\alpha'}$ operators. For brevity we will write the system in the form $A\vec{c} = \vec{b}$.

The numerical method we have chosen to solve this system is the generalized minimum residual algorithm (GMRES) [28]. GMRES is a prototype of the so-called Krilov subspaces projection methods. Its aim is to minimize the residue $\vec{r} = \vec{b} - A\vec{c}$ of an approximate solution $\vec{c}$, starting from a trial vector $\vec{c}_0$ and looking for its correction $\vec{c} - \vec{c}_0$ in the Krilov subspace $\mathcal{K} = \{\vec{r}_0, A\vec{r}_0, A^2\vec{r}_0, \ldots, A^{p-1}\vec{r}_0\}$ such that the residue $\vec{r}$ is orthogonal to $\mathcal{L} = A\mathcal{K}$. When the dimension p increases, the residue of the approximate solution $\vec{c}$ can be brought to an arbitrary small value, called tolerance. In most of the practical cases, a tolerance between 10^{-3} and 10^{-6} is sufficient.

GMRES is a powerful tool when the problem is well conditioned, which is almost never true in a realistic case. The way out is to ''precondition'' the system, i.e., to solve the equivalent problem $M^{-1}A\vec{c} = M^{-1}\vec{b}$ instead of $A\vec{c} = \vec{b}$. The closer to A the matrix M is, the better the preconditioning. Our choice was to take the matrix M equal to D. As pointed out in Refs. [24,29,1] its tensor structure, optimized by the choice of Cartesian coordinates, allows an easy inversion. Our preconditioning technique gives us a converged result after $\simeq 30$ matrix applications, for all the considered physical cases and independently of the dimension of the matrix. Examples of convergence curves, i.e., the evolution of the residue modulus at each step, are shown in Fig. 5.

In the case of the bound state, the asymptotic behavior of the wave function and FY amplitudes leads to a singular system $D(E)\vec{c} = [F+G+H]\vec{c}$ that will be rewritten for convenience in the form $A'\vec{c} = E\vec{c}$, the energy E being an eigenvalue. It is well known that iterative methods are appropriate for extracting a few eigenvalues, but only those with largest modulus. With the three-dimensional boxlike boundary condition (23), the existence of overwhelming highly positive eigenvalues leaves no hope of obtaining directly the binding energy.

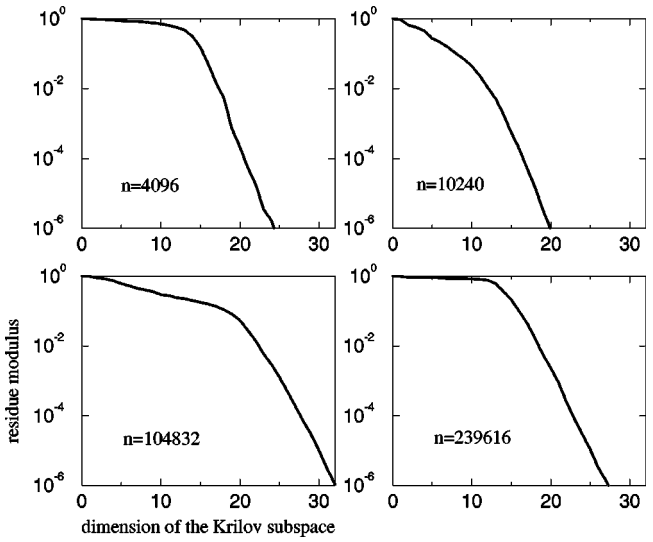

FIG. 5. Residue modulus obtained with GMRES vs the dimension of the Krilov subspace, i.e., the number of matrix applications, for different numbers n of unknowns. The linear system $A\vec{c} = \vec{b}$ is normalized such that $\|\vec{b}\| = 1$. The initial guess is chosen to be $\vec{0}$.

A crafty trick is to solve the eigenproblem $D^{-1}(E)[F+G+H]\vec{c} = \lambda\vec{c}$, where E is now a parameter [30,24]. The value E will be an eigenvalue of the initial problem when the spectrum $\{\lambda\}$ contains 1. Furthermore, it can be shown by variational considerations that the more excited the state (including the nonphysical box states), the smaller the corresponding λ. Thus the eigenvalues of physical interest can be obtained with methods like the implicit restarted Arnoldi algorithm (IRA) [31]. We notice that the full inversion of D, including the two-body potential, gives a better conditioned spectrum $\{\lambda\}$ than an inversion of its kinetic term alone, and avoids some of the awkward negative eigenvalues generated by the repulsive part of the potential. IRA is a generalization of the power method and gives the first eigenvalue in 10–15 matrix applications. It is also based on Krilov subspaces, and approximates the eigenvalues of A' by those of the restriction of A' to the space spanned by k vectors $\vec{x}_0, \vec{x}_1, \ldots, \vec{x}_{k-1}$, $\vec{x}_0$ being a trial arbitrary vector. Nevertheless, this method requires several calculations for different values of the energy and becomes numerically unstable when using highly repulsive two-body potentials, such as the interatomic ^{4}He-^{4}He one [32].

A more robust technique was finally adopted, often referred to as shift-invert method. The initial problem is written in the form $(A'-E_0)^{-1}\vec{c} = \xi\vec{c}$ and this technique converges to the energy closest to E_0. It gives very good results with a well-balanced mixture of IRA and GMRES. IRA is used to quickly obtain the dominant eigenvalue ξ_0 and provides the energy $E = E_0 + 1/\xi_0$. The real difficulty lies in the generation of the corresponding Krilov subspace. It is obviously impossible to invert $(A'-E_0)$ since the F, G, H matrices are contained in A'. The step $\vec{x}_{k+1} = (A'-E_0)^{-1}\vec{x}_k$ is then performed by a GMRES resolution of the equivalent linear system $(A'-E_0)\vec{x}_{k+1} = \vec{x}_k$. This technique presents considerable interest especially for excited states which are easily obtained, independently of the previous convergence of the less excited ones.

TABLE II. Binding energies (MeV) and rms radius (fm) for the $4N$ ground (^{4}He) and first excited (^{4}He*) states. Our results for the ^{4}He binding energy agree very well with the best existing calculations. The triton parameters are also mentioned for completeness.

	^{4}He [1]	^{4}He [34]	^{4}He	^{4}He*	^{3}H
B	30.31	30.29	30.30	8.79	8.53
rms			1.44	4.95	1.72

IV. RESULTS

The results presented in this section have been obtained with the spin-dependent S-wave interaction MT I–III:

$$V^{\sigma}(r)=V_r\frac{\exp(-\mu_r r)}{r}-V_a\frac{\exp(-\mu_a r)}{r}.$$

The potential parameters and the value $\hbar^2/m=41.47$ MeV fm^2 are the same as those used, e.g., in Refs. [1,33,34] and are slightly different from those given in the original version [30]. Despite its bare simplicity, this potential turns out to be very efficient in describing the bulk of low-energy properties in the few-nucleon systems. We will first examine what we call the S-wave approximation, i.e., the fact that aside from the zero angular momentum of the interaction pair, all the angular momenta variables in expansion (19) are set equal to zero. The convergence with respect to the l_y, l_z expansion will be examined in a second step.

A. Bound states

In the $4N$ system, the bound states exist only for the $S=T=0$ channel. In the S-wave approximation the number of FY components is limited to $N_c=4$ ($N_K=N_H=2$) (see Table I). The binding energies and rms radius for the ground (^{4}He) and first excited (^{4}He*) states are given in Table II. The corresponding grids are G_1 with $N_g=12$ and G_1^* with $N_g=6$, given in Table III. The estimated accuracy in the binding energies is 0.01 MeV but we notice that much less expensive calculations can provide a precise result as well; e.g., the grid G_2 with $N_g=8$ gives also a binding of 30.30 MeV. In the ground state we remark that there is good agreement with the best existing calculations [1,34].

TABLE III. Grids used for $4N$ ground (^{4}He) and first excited (^{4}He*) states.

				grid G_1					
x	20	1.30	10.0						
y	15	1.25	12.0						
z	15	1.25	15.0						
				grid G_2					
x	15	1.30	10.0						
y	10	1.25	12.0						
z	10	1.25	15.0						
				grid G_1^*					
x	08	1.30	08.0	05	1.10	20.0			
y	07	1.30	10.0	05	1.10	30.0			
z	07	1.20	10.0	13	1.10	80.0	10	1.00	150.0

The first excitation which, experimentally, corresponds to a $J^{\pi}=0^+$ resonance 0.40 MeV above the $p+t$ threshold [35], appears in this model as a loosely bound state. The binding energy with respect to the $N+NNN$ threshold ($E=-8.535$ MeV in this model) is 0.257 MeV. A similar result was found in Ref. [7] in which different versions of the one term separable Yamaguchy potential gives a binding energy varying from 0.07 to 0.40 MeV, depending on their different D-state contributions. This 0^+ first excitation has been widely considered in the literature as being a breathing mode [36–38]. Our conclusion is, however, different. We have calculated the regularized two-body correlation functions defined by

$$C_{\alpha_x}(x)=\sum_{\alpha'(\alpha'_x=\alpha_x)}\int\int dydz|\Psi_{\alpha'}(x,y,z)|^2, \qquad (31)$$

where $\Psi_{\alpha'}(x,y,z)$ represents the total wave function component in the α' quantum numbers, and where α_x denotes the subset of quantum numbers α relative to the x variable $(l_x,\sigma_x,j_x,\tau_x)$. The summation in Eq. (31) is performed onto one of the two bases, K or H. Once the total wave function is normalized, the correlation functions are normalized according to

$$\sum_{\alpha_x}\int dxC_{\alpha_x}(x)=1. \qquad (32)$$

The results are displayed in Fig. 6. The separated contributions from the singlet and triplet state are plotted for (a) triton, (b) ^{4}He ground state, and (c) ^{4}He first excited state. The difference between the correlation functions for the ground and excited states is remarkable, both in the shape and in the separated singlet-triplet contributions. For the excited state one can distinguish the superposition of two structures with two different length scales, the short-distance part being similar to the triton one. This suggests a $1+3$ structure for the ^{4}He excited state, as can be more clearly seen in plot (d) where the results of (c) are compared with those of the triton suitably normalized. Contrary to what would happen in a breathing mode, the short distance behavior of the nucleons is that of an unperturbed triton with the fourth nucleon being simply a remote spectator.

By modifying the MT I–III potential strength we failed to pull the state out of the bound region, the three-body threshold moving in the same direction. It seems very difficult for a pure strong interaction to generate a first excitation in the continuum. The right position of this resonance is, however, a crucial point in any attempt to describe the low-energy data (e.g., $p+t$) [20]. The effect of Coulomb interactions could be enough. However, the inclusion of an *ad hoc* repulsive four-body term $V(\rho)=V_0e^{-\rho^2}$ can also achieve the same result.

The preceding results are only slightly modified by the inclusion of higher partial waves in the FY expansion. The effects of these contributions can be seen in Table IV. Their smallness shows the validity of the S-wave approximation. These results have been obtained using the grid G_2 with

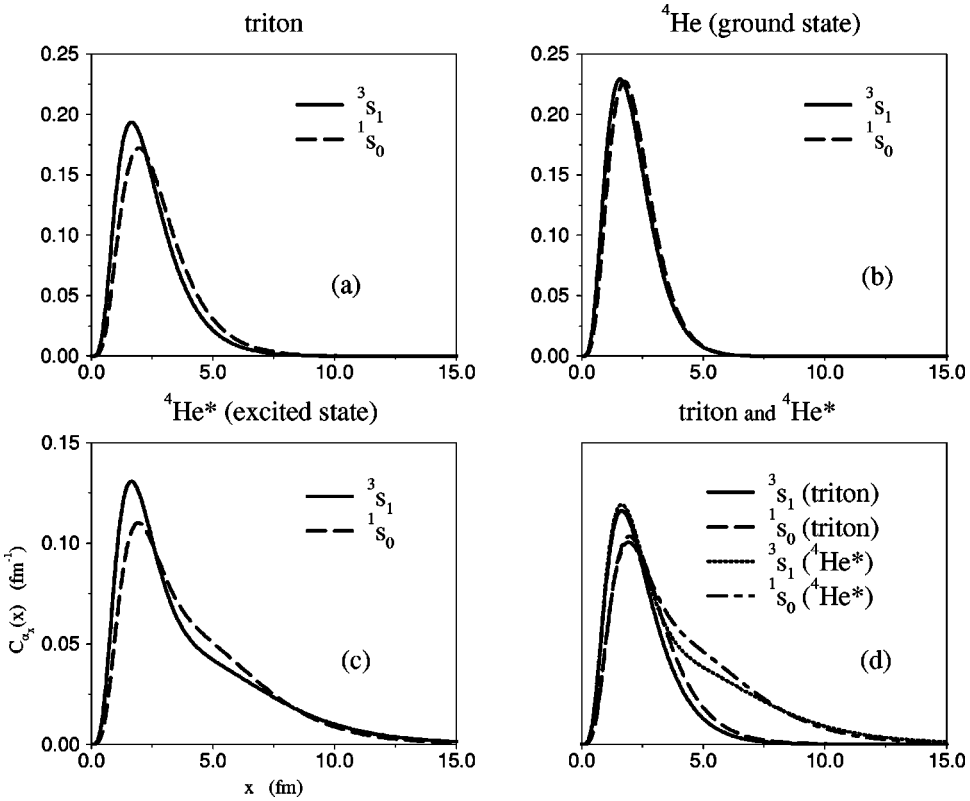

FIG. 6. Two-body correlation functions $C_{\alpha_x}(x)$ for (a) triton, (b) ^{4}He ground, and (c) first excited states. Solid (dashed) line denotes the triplet (singlet) contributions. In (d), the results of ^{4}He first excited state are compared to the triton correlation function suitably scaled.

$N_g=8$ for the ground state and G_1^* with $N_g=6$ for the first excitation for which the corresponding triton binding energy is $B_3=8.513$ MeV.

B. Elastic $N+NNN$ scattering

A crucial point in our method is to ensure the proper description of the $3N$ asymptotic state. This is used to fix the grid parameters for the x,y variables. In order to exhibit the stability of our results, we will compare the phase shifts obtained with several tritons corresponding to increasing numerical accuracies. The considered grids, detailed in Table V, are T_4 with $N_g=6$ and a binding energy $B=8.593$ MeV, T_8 with $N_g=8$ and $B=8.527$ MeV, and T_{10} with $N_g=8$ and $B=8.535$ MeV. We recall that the precise value for the $3N$ binding energy is $B=8.535$ MeV. The grid parameters for the z variable depends substantially on the relative kinetic energy. A zero energy calculation requires a relatively large value of z_N but very few points inside are sufficient to describe an asymptotic linear behavior. On the contrary as far as the energy increases, the value of z_N can be decreased but the oscillations in the relative wave functions demand an increasingly big number of points. A typical grid for the case $E=0$ is $G_z\equiv\{10,1.20,19.0;03,1.00,34.0\}$.

TABLE IV. Nonzero angular momentum contributions to ^{4}He and ^{4}He* binding energies.

N_K+N_H	l_x	l_y	l_z	B_4	B_4^*	B^*-B_3
2+2	0	0	0	30.302	8.769	0.257
8+2	0	0,1	0,1	30.319	8.763	0.250
16+3	0	0,1,2	0,1,2	30.324	8.770	0.257

We have shown in Table VI the phase shifts for different (S,T) channels as a function of the center of mass energy. For all of them, we have arbitrarily chosen, as in Ref. [5], the determination $\delta(E=0)=180°$. For the $S=0$ case the comparison between grids T_4 and T_8 has been made, showing a good stability despite the fact that grid T_4 gives only a poor description of the asymptotic state. As it has been already emphasized in Sec. II, the key point in our approach to the scattering problem lies in the coherence between the asymptotic state and the numerical solution of the $4N$ problem, rather than in a very precise description of it. The results corresponding to grid T_8 are considered as converged.

A zero energy calculation directly provides us with the scattering length. The results, given in Table VII, show a high stability with respect to grid variations (T_8 and T_{10}) and our estimated accuracy is given in column 3. These values are in agreement with the existing published calculations [13]. For $T=1$ they are close to those obtained in Ref. [5]

TABLE V. The grids T_4, T_8, T_{10} used for the tritons 4, 8, 10.

grid T_4: $B_3=8.593$ MeV						
x	08	1.30	14.0	01		18.0
y	07	1.20	19.0	02	1.00	29.0
grid T_8: $B_3=8.527$ MeV						
x	12	1.30	14.0	01		18.0
y	10	1.20	19.0	02	1.00	29.0
grid T_{10}: $B_3=8.535$ MeV						
x	18	1.20	14.0	02	1.00	18.0
y	15	1.10	19.0	04	1.00	29.0

TABLE VI. $N+NNN$ phase shifts (deg), as a function of the center of mass kinetic energy (MeV), in different (S,T) channels. In the $S=0$ case, the results with different grids are shown.

E_c (MeV)	δ (deg.)	
$S=0,\ T=1$	T_4	T_8
0.05	169.97	169.95
0.1	165.85	
0.5	148.99	
1.0	137.13	137.07
2.0	121.79	
3.0	111.27	
4.0	102.93	102.82
5.0	96.18	96.13
6.0	90.18	90.24
$S=0,\ T=0$	T_4	T_8
0.01	165.17	164.05
0.02	159.17	157.66
0.05	147.73	
0.07	142.29	
0.1	135.72	132.98
0.2	120.52	
0.3	109.52	106.95
0.5	95.81	
0.7	85.57	
1.0	74.08	71.05
2.0	49.92	47.16
3.0	34.71	32.07
4.0	23.60	21.04
$S=1,\ T=1$		T_8
0.03		172.97
0.06		170.07
0.12		166.0
0.3		158.02
0.9		142.84
1.8		129.11
2.7		119.43
3.6		111.84
5.4		100.10
6.3		94.84
$S=1,\ T=0$		T_8
0.01		176.46
0.02		174.99
0.05		172.09
0.1		168.83
0.5		155.23
1.0		145.35
2.0		132.06
3.0		122.53
4.0		114.96
5.0		108.68
6.0		103.24

TABLE VII. $N+NNN$ scattering lengths values in different (S,T) channels, in the S-wave approximation.

		a_{ST} (fm)				
S	T	triton 8	triton 10	final value		
0	1	4.13	4.13	4.13	$\pm$	0.01
1	1	3.73	3.73	3.73	$\pm$	0.01
0	0	14.78	14.76	14.76	$\pm$	0.02
1	0	3.25	3.25	3.25	$\pm$	0.01

although with the original potential parameters.

The remaining low-energy parameters have been extracted from the phase shifts and are given in Table VIII for the different (S,T) channels. They are defined in the effective range expansion,

$$g_0(q)=q\ \cot\ \delta(q)=\chi(q)\left[-\frac{1}{a}+\frac{1}{2}r_0q^2+v_0q^4\right], \quad (33)$$

where $\chi(q)=1$ in the usual case but has to be modified in the presence of a near threshold singularity. According to Ref. [39], we have taken the form (q_0 real)

$$\chi(q)=\frac{1}{1-(q/q_0)^2}. \quad (34)$$

The validity of the expansion (33) in the energy region below the first inelastic threshold is displayed in Fig. 7. The usual effective range approximation, i.e., $\chi(q)=1$ and the q^4 contribution neglected in Eq. (33), works very well in the whole energy domain for all but the $(S=0,\ T=0)$ channel, in which the existence of a near threshold ^{4}He excited state requires the explicit inclusion of the pole contribution (34). It is worth noticing that the contributions coming from the v_0 term are very small and have been included only for completeness. On the contrary the pole contribution, existing only in the $(S=0,\ T=0)$ channel, is essential. Expansion (33) provides a very accurate parametrization of the S-wave scattering amplitude in all the energy region below the breakup threshold.

We would like to emphasize here the coherence between the ^{4}He* and the scattering results in the $(S=0,\ T=0)$ channel. Inserting the effective range expansion (33) in the S-wave scattering amplitude

$$f_0(q)=\frac{1}{g_0(q)-iq}$$

produces an imaginary pole in the upper complex q plane with value $q^*=0.095i$. The corresponding energy E^*

TABLE VIII. Low-energy $N+NNN$ parameters, in the S-wave approximation.

S	T	a (fm)	r_0 (fm)	v_0 (fm^3)	q_0 (fm^{-1})	a [13]
0	1	14.75	6.75	0.462		
1	1	3.25	1.82	0.231		
0	0	4.13	2.01	0.308	0.505	4.0
1	0	3.73	1.87	$\simeq 0$		3.6

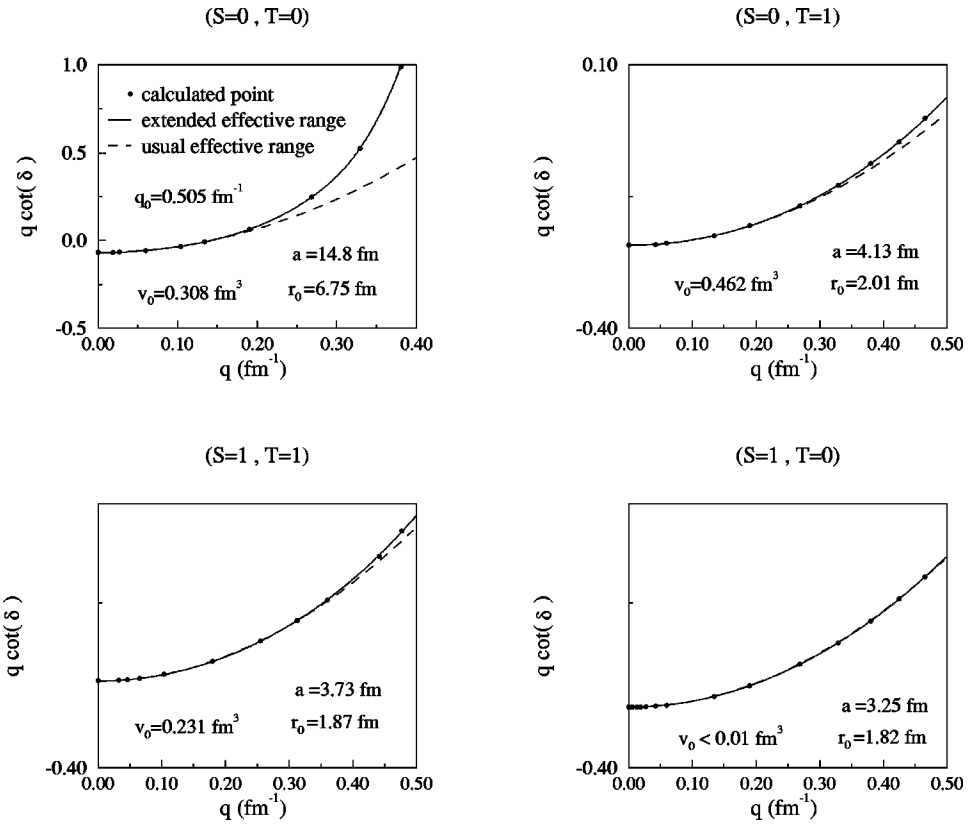

FIG. 7. Effective range expansion, q being the center of mass momentum. The usual one (dashed curve) gives a quite accurate description of the scattering amplitude, except in the ($S=0$, $T=0$) case. The full expansion (33) (solid line) provides a perfect fit of the calculated points.

$=\frac{2}{3}\hbar^2 q^{*2}/m=0.25$ MeV is in close agreement with the direct calculation given in Table II.

A step beyond the S-wave approximation has been taken by keeping the S-wave interaction alone but allowing nonzero values in the angular momentum expansion of the FY amplitudes. Table IX shows the sensibility of the scattering lengths values when the maxima of l_y and l_z vary from 0 to 2. In the particular interaction model we are considering, the number of channels describing the $3N$ asymptotic state remains the same whereas the number of channels N_c of the $4N$ problem considerably increases. These results have been obtained with the grid T_8 and $N_g=8$ completed with a suitable z grid. The values are well converged with $l_y, l_z=0,1$ except in the ($S=0$, $T=0$) case, where the big value of the scattering length makes this state rather sensitive to small parameter variations.

The $n+t$ cross section. Of particular interest is to apply the preceding results to the description of $n+t$ cross section.

TABLE IX. Convergence of low energy $N+NNN$ scattering lengths, with respect to increasing internal angular momenta.

S	T	$l_y, l_z=0$		$l_y, l_z=0,1$		$l_y, l_z=0,1,2$		$l_y, l_z=0,1,2,3$	
		a	N_c	a	N_c	a	N_c	a	N_c
0	0	14.78	4	14.86	10	14.72	16	14.72	22
1	0	3.25	4	3.08	17	3.08	31	3.08	45
0	1	4.13	4	4.10	12	4.10	20	4.10	28
1	1	3.73	6	3.63	23	3.63	41	3.63	59

On the one hand this is a pure $T=1$ channel, free from the difficulties related to the Coulomb interactions. On the other hand, accurate low-energy scattering data exist [40], showing a structure at neutron laboratory energy $T_{\rm lab}\approx 4$ MeV which is supposed to be created by a series of P-waves resonances [35]. The calculations discussed in the preceding section have thus been completed up to the first three-body breakup threshold by the inclusion of the first negative parity states $J^\pi=0^-,1^-,2^-$ corresponding to $n+t$ relative P waves. The resulting total cross sections are plotted in Fig. 8. The contributions from $n+t$ relative S and P waves are distinguished. We notice that the MT I–III model conserves separately L and S and consequently the $J^\pi=0^-,1^-,2^-$ states coming from $L=1$, $S=1$ are degenerate. The corresponding cross sections differ only by statistical factors. The remaining $J^\pi=1^-$ state comes from an $L=1$, $S=0$ coupling. In view of these results, several remarks are in order.

(1) The scattering lengths obtained in the S-wave approximation (Table VII) gives a slightly overestimated value for the zero energy cross section $\sigma(0)=1.85$ b. The experimental extrapolated zero energy cross section is $\sigma(0)=1.70\pm0.03$ b [40,41]. However, the inclusion of higher partial waves in the FY expansion (Table IX) significantly reduces the S-wave approximation result to $\sigma(0)=1.77$ b in closer agreement with experiment.

(2) The comparison of the separated spin contribution is not possible since the values of the spin-dependent scattering lengths, summarized in Table X, are still controversial.

(3) Despite the simplicity of this model, the agreement with experimental data in the resonance region, is very good.

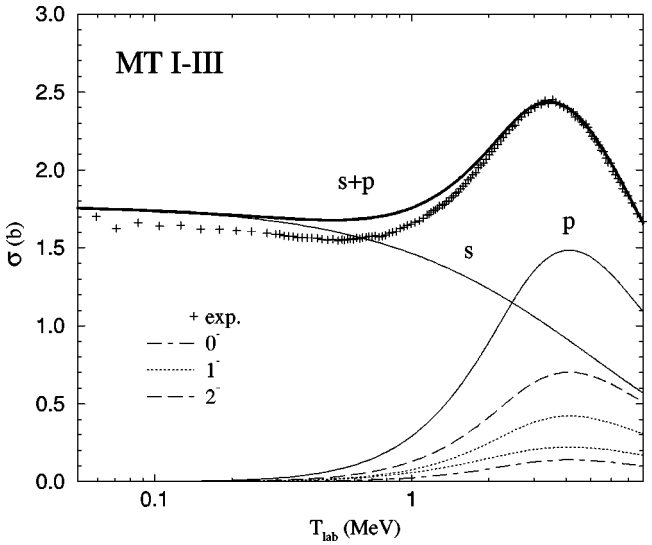

FIG. 8. The $n+t$ cross section σ calculated with MT I–III potential is compared to experimental data. The s-wave contribution (s, solid line) is slightly overestimated due to the overestimated scattering lengths. The p-wave contribution (p, solid line) dominates in the resonance region and is responsible for the very nice agreement ($s+p$ thick line) with the experimental total cross section (crosses). The $L=1$, $S=1$ contribution is split by statistical factors into its $J^\pi=0^-,1^-,2^-$ components (dot-dashed, dotted, dashed curves), whereas the $L=1$, $S=0$ one corresponds to a pure $J^\pi=1^-$ (dotted curve) partial wave.

The $n+t$ P-wave resonances are generated by an NN S-wave interaction alone. An effective $1+3$ P-wave potential is created due to the exchange mechanism between the four nucleon. We remark, however, that a first attempt to describe this cross section with $l_z=1$ in the K components but keeping zero all the remaining angular momenta in Eq. (19) failed. The incoming neutron seems thus to be more sensible to the virtual excitations of the triton than to the NN pair interactions themselves.

(4) We have calculated the contribution coming from the $n+t$ relative D waves. They are given by the positive parity states $L=2$, $S=0,1$. The corresponding phase shifts at 6 MeV c.m. kinetic energy are $\delta_{S=0}=-3.3°$ and $\delta_{S=1}=-2.4°$, which contributes only a few mb to the total cross section. The results displayed Fig. 8 can so be considered as fully converged in the MT I–III model.

C. First inelastic channel

The last point to be presented in this work concerns the reaction

TABLE X. Latest experimental results concerning $n+t$ singlet (a_0) and triplet (a_1) scattering lengths (in fm).

a_0			a_1			
3.91	±	0.12	3.6	±	0.1	[40]
4.98	±	0.29	3.13	±	0.11	[43]
2.10	±	0.31	4.05	±	0.09	[43]
4.453	±	0.10	3.325	±	0.016	[44]

$$p+{}^3\mathrm{H}\rightarrow p+{}^3\mathrm{H}$$
$$\rightarrow n+{}^3\mathrm{He}$$
$$\rightarrow d+d.$$

In the isospin approximation employed throughout this work, both $n+{}^3$He and $p+t$ thresholds are degenerate and correspond to the $N+NNN$ of the preceding section. The Pauli principle imposes for the deuteron-deuteron channel $(-)^{L+S+T}=+1$. If we assume the final state $d+d$ to be in a relative S wave one has $L=T=0$ and $J^\pi=0^+,2^+$. The $J^\pi=2^+$ state requires a relative angular momentum $l_z=2$ in the initial $N+NNN$ channel and it is expected to give small contribution at very low $d+d$ energy. We will consider only the $(J^\pi=0^+,\ T=0)$ state.

The S matrix is defined according to Eq. (28). We present in Table XI the S-matrix elements at several energies, chosen with respect to the $NN+NN$ threshold. $N+NNN$ is referred to as channel 1, $NN+NN$ as channel 2. The symmetry and unitarity properties are there fulfilled at the level of 10^{-3}, which corresponds to the accuracy of our results.

With the conventions used above, the scattering cross sections in a given partial wave (J^π) in presence of several channels $a,a',\ldots$, are given by

$$\sigma^{(J)}_{a\rightarrow a}=\frac{\pi}{q_a^2}\frac{\hat{J}}{\widehat{S_{a_1}}\cdot\widehat{S_{a_2}}}|1-S_{aa}|^2, \tag{35}$$

$$\sigma^{(J)}_{a\rightarrow a'}=\frac{\pi}{q_a^2}\frac{\hat{J}}{\widehat{S_{a_1}}\cdot\widehat{S_{a_2}}}|S_{a'a}|^2, \tag{36}$$

where the notation $\hat{J}$ holds for $2J+1$. S_{a_i} denotes the spin of the colliding cluster a_i. The corresponding values with $a,a'\equiv N+NNN,NN+NN$ are given in Fig. 9 (filled circles). We remark no accident in the $N+NNN$ cross section when the inelastic $NN+NN$ threshold is open. The $NN+NN\rightarrow N+NNN$ cross section displays the usual $1/v$ law of the inelastic process and the crossed channel $N+NNN\rightarrow NN+NN$ the expected $\sqrt{E}$ law. The elastic $d+d$ cross section has been calculated neglecting Coulomb interactions which will make this quantity divergent. However, due to the absence of nearthreshold singularity, one can expect small corrections to the low-energy parameters obtained in this way, as in the $n+n$ versus $p+p$ case.

Of particular interest is the extraction of the imaginary part of the strong $d+d$ scattering length, a quantity which controls the fusion rate in the process $d+d\rightarrow n+{}^3$He. This can be done either from the linear behavior of the $d+d$ phase shifts $\delta_{22}=-(a_R-ia_I)q_2$ (with $S_{22}=e^{2i\delta_{22}}$), as displayed in Fig. 10, or from the inelasticity in the nondiagonal S-matrix element which behaves as $|S_{12}|^2=-4a_Iq_2(1+2a_Iq_2)$. Both methods agree with high accuracy and lead to the following values:

$$a_R=+4.91\pm0.02\ \text{fm}, \tag{37}$$

$$a_I=-0.0115\pm0.0001\ \text{fm}. \tag{38}$$

TABLE XI. $N+NNN \leftrightarrow NN+NN$ S-matrix elements. The $N+NNN$ channel is labeled by 1, the $NN+NN$ one by 2.

E_c c.m. (MeV)		S matrix			
$N+NNN$	$NN+NN$	S_{11}	S_{12}	S_{21}	S_{22}
4.1253	0.05	$0.772+0.634i$	$-0.00473+0.0472i$	$-0.00471+0.0470i$	$0.882-0.468i$
4.1753	0.10	$0.782+0.621i$	$0.000488+0.0564i$	$0.000486+0.0563i$	$0.771-0.634i$
4.2753	0.20	$0.802+0.594i$	$0.0110+0.0661i$	$0.0110+0.0661i$	$0.566-0.821i$
4.3253	0.25	$0.811+0.581i$	$0.0160+0.0690i$	$0.0161+0.0691i$	$0.472-0.879i$
4.3753	0.30	$0.820+0.567i$	$0.0209+0.0711i$	$0.0210+0.0713i$	$0.382-0.921i$
4.5753	0.50	$0.854+0.514i$	$0.0391+0.0748i$	$0.0393+0.0752i$	$0.0659-0.994i$
5.0753	1.00	$0.919+0.381i$	$0.0759+0.0679i$	$0.0758+0.0678i$	$-0.480-0.871i$
5.5753	1.50	$0.961+0.253i$	$0.103+0.0508i$	$0.102+0.0506i$	$-0.784-0.610i$
6.0753	2.00	$0.983+0.133i$	$0.120+0.0292i$	$0.123+0.0301i$	$-0.934-0.335i$

We remark that a very small value of a_I which should be only slightly modified once the Coulomb interaction is switched on. This small value is due to the small overlapping between the K and H configurations which respectively govern the $N+NNN$ and $NN+NN$ asymptotic states.

V. CONCLUSION

We have presented the first solution of Faddeev-Yakubovsky equations in configuration space for the scattering states in the $4N$ system. They concern both the $N+NNN$ elastic scattering and its coupling to the first inelastic $NN+NN$ channel. The results presented here have been obtained with an S-wave model interaction and in the isospin symmetry approximation, i.e., neglecting the Coulomb and mass difference effects.

The $N+NNN$ elastic phase shifts have been calculated for the different spin and isospin channels. The low-energy parameters have been extracted and the validity of the effective range approximation in the energy region below the three-body break-up threshold has been analyzed. We have in particular found the importance of including the pole contribution in the $(S=0,\ T=0)$ case due to the vicinity of the first $J^\pi=0^+$ excitation. We have also found that in the framework of our model this 0^+ state is bound at 0.25 MeV below the $3N$ threshold. The study of the two-body correlation functions showed that the structure of this state is a $1+3$ configuration rather than a breathing mode, as is usually accepted. The coherence between the binding energy of this state and the scattering results has been emphasized.

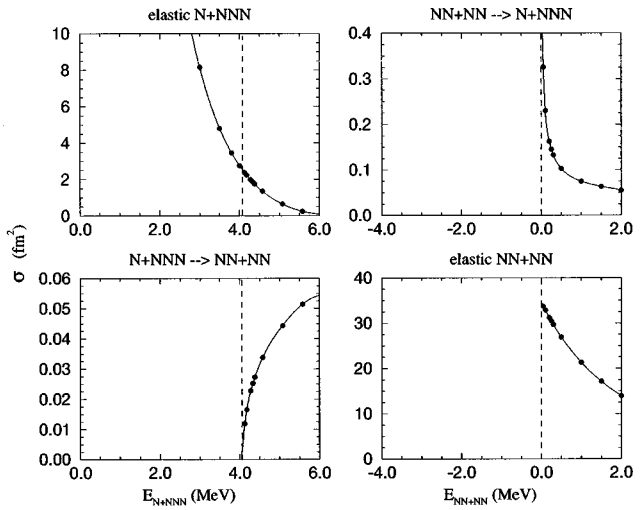

FIG. 9. Elastic and inelastic cross sections (solid curves), in fm^2, for the coupled channels $N+NNN$-$NN+NN$. They are interpolated between the calculated values (filled circles). The energies are given in the center of mass of the incident channel.

The $n+t$ scattering cross section has been treated with a special interest and the first negative parity states have been included, to account for the structure experimentally observed. The elastic cross section is well described by the simple MT I–III interaction, especially in the resonance region. The $n+t$ P-wave resonance is thus reproduced by a NN pure S-wave interaction. This shows the difficulty to understand this structure in terms of the NN interaction alone. It is created by the direct and exchange mechanism between the incoming neutron and the target nucleons.

The S matrix coupling the $N+NNN$ and $NN+NN$ channels has been obtained as well as the corresponding cross sections. The analysis of these results allows the extraction of the $NN+NN$ scattering length, whose imaginary part controls the fusion process $d+d \rightarrow n+{}^3\mathrm{He}$. Its value turned out to be very small ($a_I \simeq 0.011$ fm). Further applications of this formalism including Coulomb interactions and more realistic potentials are in process.

ACKNOWLEDGMENTS

We are indebted to Professor C. Gignoux for his continuous teaching and helpful discussions during the elaboration of this work. The numerical calculations were initiated on the Cray-T3D/T3E at the CGCV (Centre Grenoblois de Calcul Vectoriel, CEA), and completed on the Cray-T3E at the IDRIS (Institut du Développement et des Resources en Informatique Scientifique, CNRS). We are grateful to the staff members of these two organizations for their kind hospitality and useful advice.

APPENDIX

This appendix aims at the complete expression of the functions f,g,h appearing in Eq. (21) in terms of the corresponding quantum numbers α and α'. By projection onto the

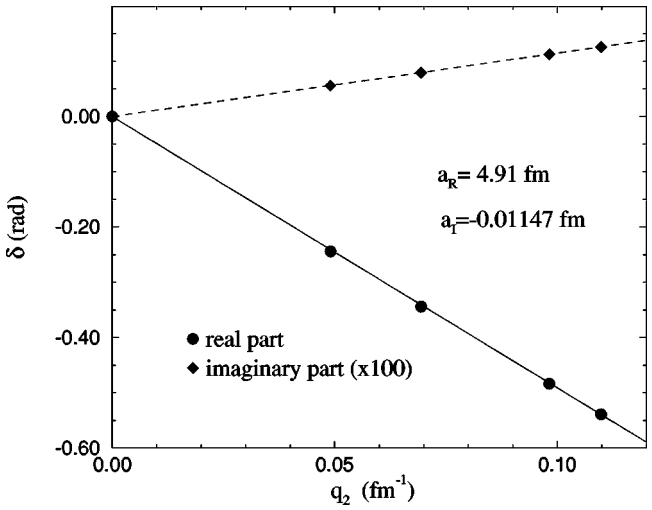

FIG. 10. Low-energy behavior of the deuteron-deuteron phase shift δ and determination of the scattering length. Its real or imaginary parts a_R or a_I are deduced from the proportionality between the real (solid curve) or imaginary (dashed curve) parts of the phase shift and the center-of-mass momentum q_2.

appropriate K and H basis, the right-hand side of Eqs. (11) gives raise to integral terms as shown in Eq. (13), involving some very complicated functions f,h,g, generated by permutations operators.

1. Permutation operators

The permutation operators P_{ij} are completely defined by their action upon each ket of a complete basis. This basis is chosen to be an ordered quadruplet $|q_1q_2q_3q_4\rangle$, where the given ith value represents the state of the ith particle, including the space, spin, and isospin degrees of freedom. This basis is a generalization of the one given in Eq. (10). It is assumed that P_{ij} corresponds to an exchange between the ith and jth set of quantum numbers, e.g.,

$$P_{34}|q_1q_2q_3q_4\rangle=|q_1q_2q_4q_3\rangle.$$

More complex permutations are then transparent, e.g.,

$$P_{23}P_{34}|q_1q_2q_3q_4\rangle=|q_1q_4q_2q_3\rangle.$$

The way the permutation operators act upon the coupled bases (K or H) can be deduced from this basic feature. In the configuration space, e.g., a single operator results in a generalized rotation of the Jacobi coordinates. Note that because of the symmetry of the bases, the contribution of the operators P_{13}, $P_{13}P_{34}$, and $P_{14}P_{23}$ are identical to those of P_{23}, $P_{23}P_{34}$, and $P_{13}P_{24}$.

2. $\mathcal{H}$ functions

All the permutation operations can be seen as, at most, two successive rotations, each of them involving only two coordinates, e.g., first of all y and z, then x and one of the preceding rotated coordinates. So it is convenient to use the functions appearing in the three-body problem [42], defined as follows.

Suppose we are to calculate the projection of a given expression $[Y_{l_x'}(\hat{x}')Y_{l_y'}(\hat{y}')]_L F(x',y')$, F being an arbitrary function of x' and y', onto a bipolar-harmonic basis $[Y_{l_x}(\hat{x})Y_{l_y}(\hat{y})]_L$, where the following relation holds:

$$\begin{pmatrix}\vec{x}'\\ \vec{y}'\end{pmatrix}=\begin{pmatrix}a & b\\ c & d\end{pmatrix}\begin{pmatrix}\vec{x}\\ \vec{y}\end{pmatrix}. \tag{A1}$$

We define $\mathcal{H}$ functions such that

$$\int\int d\hat{x}d\hat{y}[Y_{l_x}(\hat{x})Y_{l_y}(\hat{y})]_L^*[Y_{l_x'}(\hat{x}')Y_{l_y'}(\hat{y}')]_L F(x',y')$$
$$=\frac{1}{2}\int_{-1}^{1}du\mathcal{H}^L_{l_xl_y,l_x'l_y'}(x,y,u)F(x',y'),$$

where, in the integral term, x' and y' are obtained from Eq. (A1) with the constraint $\cos(\widehat{\hat{x},\hat{y}})=u$. These functions are given, for example, by

$$\mathcal{H}^L_{l\lambda,l'\lambda'}(x,y,u)=\sum_{k,l_1,l_2,\lambda_1,\lambda_2,l_0,\lambda_0(l_1+l_2=l',\lambda_1+\lambda_2=\lambda')}(-)^{l'+\lambda'+L+k}\cdot a^{l_1}b^{l_2}c^{\lambda_1}d^{\lambda_2}\hat{l}'\hat{\lambda}'\hat{k}\hat{l}_0\hat{\lambda}_0$$
$$\times\sqrt{\frac{(2l')!(2\lambda')!\hat{l}\hat{\lambda}}{(2l_1)!(2l_2)!(2\lambda_1)!(2\lambda_2)!}}\begin{pmatrix}k & l_0 & l\\ 0 & 0 & 0\end{pmatrix}\begin{pmatrix}k & \lambda_0 & \lambda\\ 0 & 0 & 0\end{pmatrix}\begin{pmatrix}l_1 & \lambda_1 & l_0\\ 0 & 0 & 0\end{pmatrix}$$
$$\times\begin{pmatrix}l_2 & \lambda_2 & \lambda_0\\ 0 & 0 & 0\end{pmatrix}\begin{Bmatrix}\lambda & l & L\\ l_0 & \lambda_0 & k\end{Bmatrix}\begin{Bmatrix}l_1 & l_2 & l'\\ \lambda_1 & \lambda_2 & \lambda'\\ l_0 & \lambda_0 & L\end{Bmatrix}\frac{x^{l_1+\lambda_1}y^{l_2+\lambda_2}}{(x')^{l'}(y')^{\lambda'}}P_k(u),$$

where $\hat{l}=2l+1$ and P_k stands for the kth-Legendre polynomial.

Obviously, in the four-body case, one has to deal with cumbersome recoupling, to isolate bipolar harmonics from the more complex coupling scheme (20). Nevertheless all the work can be built upon this basic function.

3. The only nonzero f function

$f_{\alpha,\alpha'}$ is nonzero when both α and α' are of H type. Let us define then $x^f_{\alpha\alpha'}$, $y^f_{\alpha\alpha'}$, $z^f_{\alpha\alpha'}$ by

$$\begin{pmatrix} \vec{x}^f_{\alpha\alpha'} \\ \vec{y}^f_{\alpha\alpha'} \\ \vec{z}^f_{\alpha\alpha'} \end{pmatrix} = \begin{pmatrix} 0 & 1 & 0 \\ 1 & 0 & 0 \\ 0 & 0 & -1 \end{pmatrix} \begin{pmatrix} \vec{x} \\ \vec{y} \\ \vec{z} \end{pmatrix}.$$

$f_{\alpha,\alpha'}$ is given by

$$f_{\alpha,\alpha'} = t_{\alpha,\alpha'} \delta_{l_z,l'_z} \delta_{\sigma'_x,\sigma_y} \delta_{\sigma_x,\sigma'_y} \delta_{l_x,l'_y} \delta_{l'_x,l_y} \delta_{j_x,j'_y} \delta_{j'_x,j_y} \delta_{j_{xy},j'_{xy}} (-)^{j_x+j_y-j_{xy}+l_z},$$

where the isospin contribution $t_{\alpha,\alpha'}$ is $t_{\alpha,\alpha'} = \delta_{\tau_x,\tau'_y} \delta_{\tau'_x,\tau_y} (-)^{\tau_x+\tau_y-T}$.

4. *h* functions

There are two cases where the *h* functions can be nonzero when the amplitude α' is of *K* type.

a. α of K type

$x^h_{\alpha\alpha'}, y^h_{\alpha\alpha'}, z^h_{\alpha\alpha'}$ are then defined by

$$\begin{pmatrix} \vec{x}^h_{\alpha\alpha'} \\ \vec{y}^h_{\alpha\alpha'} \\ \vec{z}^h_{\alpha\alpha'} \end{pmatrix} = \begin{pmatrix} \frac{1}{2} & \frac{\sqrt{3}}{2} & 0 \\ \frac{\sqrt{3}}{2} & -\frac{1}{2} & 0 \\ 0 & 0 & 1 \end{pmatrix} \begin{pmatrix} \vec{x} \\ \vec{y} \\ \vec{z} \end{pmatrix}$$

and the complete expression for $h_{\alpha\alpha'}$ is

$$h_{\alpha,\alpha'}(x,y,z,u) = \varepsilon t_{\alpha,\alpha'} \sum_{l_{xy},\sigma} \delta_{l_z,l'_z} \delta_{j_z,j'_z} \delta_{J_3,J'_3} A \begin{Bmatrix} l_x & \sigma_x & j_x \\ l_y & s_3 & j_y \\ l_{xy} & \sigma & J_3 \end{Bmatrix} A \begin{Bmatrix} l'_x & \sigma'_x & j'_x \\ l'_y & s_2 & j'_y \\ l_{xy} & \sigma & J_3 \end{Bmatrix}$$
$$\times (-)^{s_1+s_2-\sigma_x+s_2+\sigma'_x-\sigma} A \begin{Bmatrix} s_2 & s_1 & \sigma_x \\ s_3 & \sigma & \sigma'_x \end{Bmatrix} \frac{xyz}{x^h_{\alpha\alpha'} y^h_{\alpha\alpha'} z^h_{\alpha\alpha'}} \mathcal{H}^{l_{xy}}_{l_x l_y, l'_x l'_y}(x,y,u),$$

where

$$A \begin{Bmatrix} j_1 & j_2 & j_3 \\ j_4 & j_5 & j_6 \\ j_7 & j_8 & j_9 \end{Bmatrix} = \sqrt{\hat{j}_{13}\hat{j}_6\hat{j}_7\hat{j}_8} \begin{Bmatrix} j_1 & j_2 & j_3 \\ j_4 & j_5 & j_6 \\ j_7 & j_8 & j_9 \end{Bmatrix}, \quad \hat{j} = 2j+1, \quad t_{\alpha,\alpha'} = (-1)^{t_1+t_2-\tau_x+t_2+\tau'_x-T'_3}, \quad \delta_{T_3,T'_3} A \begin{Bmatrix} t_2 & t_1 & \tau_x \\ t_3 & T_3 & \tau'_x \end{Bmatrix}$$

and with the constraint $\cos(\widehat{\hat{x},\hat{y}}) = u$.

b. α of H type

$x^h_{\alpha\alpha'}, y^h_{\alpha\alpha'}, z^h_{\alpha\alpha'}$ are now defined by

$$\begin{pmatrix} \vec{x}^h_{\alpha\alpha'} \\ \vec{y}^h_{\alpha\alpha'} \\ \vec{z}^h_{\alpha\alpha'} \end{pmatrix} = \begin{pmatrix} -\frac{1}{\sqrt{3}} & 0 & -\frac{\sqrt{2}}{\sqrt{3}} \\ 0 & 1 & 0 \\ \frac{\sqrt{2}}{\sqrt{3}} & 0 & -\frac{1}{\sqrt{3}} \end{pmatrix} \begin{pmatrix} \vec{x} \\ \vec{y} \\ \vec{z} \end{pmatrix}$$

and the corresponding expression for $h_{\alpha\alpha'}$ is

$$h_{\alpha,\alpha'}(x,y,z,u) = \varepsilon t_{\alpha,\alpha'} \sum_{l'_{yz},J'_2} \delta_{l'_x,l_y} \delta_{\sigma'_x,\sigma_y} (-)^{j_{xy}+l_z-J+j_y+J'_2-J+l_x+l_z-l'_{yz}} A \begin{Bmatrix} l_z & j_x & J'_2 \\ j_y & J & j_{xy} \end{Bmatrix} A \begin{Bmatrix} j'_x & j'_y & J'_3 \\ j'_z & J & J'_2 \end{Bmatrix} A \begin{Bmatrix} l'_y & s_1 & j'_y \\ l'_z & s_2 & j'_z \\ l'_{yz} & \sigma_x & J'_2 \end{Bmatrix}$$
$$\times A \begin{Bmatrix} l_z & l_x & l'_{yz} \\ \sigma_x & J'_2 & j_x \end{Bmatrix} \frac{xyz}{x^h_{\alpha\alpha'} y^h_{\alpha\alpha'} z^h_{\alpha\alpha'}} \mathcal{H}^{l'_{yz}}_{l_x l_z, l'_y l'_z}(x,z,u)$$

with

$$t_{\alpha,\alpha'}=\delta_{\tau_x',\tau_y}(-)^{\tau_x+\tau_y-T}A\begin{Bmatrix}\tau_x' & t_3 & T_3'\\ t_4 & T & \tau_x\end{Bmatrix}$$

and the constraint $\cos(\widehat{\hat{x},\hat{z}})=u$.

5. g functions

There are two cases where the g functions can be nonzero: the amplitude α must be of K type.

a. α' of K type

It is necessary to define in this case $x^g_{\alpha\alpha'},y^g_{\alpha\alpha'},z^g_{\alpha\alpha'}$ and an intermediate coordinate $\vec{y}_0$ such that

$$\begin{pmatrix}\vec{x}^g_{\alpha\alpha'}\\ \vec{y}^g_{\alpha\alpha'}\\ \vec{z}^g_{\alpha\alpha'}\end{pmatrix}=\begin{pmatrix}1 & 0 & 0\\ 0 & \frac{1}{3} & \frac{2\sqrt{2}}{3}\\ 0 & \frac{2\sqrt{2}}{3} & -\frac{1}{3}\end{pmatrix}\begin{pmatrix}\vec{x}^g_{\alpha\alpha'}\\ \vec{y}_0\\ \vec{z}\end{pmatrix}\quad\text{and}\quad\begin{pmatrix}\vec{x}^g_{\alpha\alpha'}\\ \vec{y}_0\\ \vec{z}\end{pmatrix}=\begin{pmatrix}\frac{1}{2} & \frac{\sqrt{3}}{2} & 0\\ \frac{\sqrt{3}}{2} & -\frac{1}{2} & 0\\ 0 & 0 & 1\end{pmatrix}\begin{pmatrix}\vec{x}\\ \vec{y}\\ \vec{z}\end{pmatrix}.$$

The corresponding expression for $g_{\alpha\alpha'}$ is

$$g_{\alpha,\alpha'}(x,y,z,u,v)=\frac{1}{2}t_{\alpha,\alpha'}\sum_{l_{xy},\sigma,l'_{xy},\sigma',l'_{yz},L,S,\lambda}A\begin{Bmatrix}l_x & \sigma_x & j_x\\ l_y & s_3 & j_y\\ l_{xy} & \sigma & J_3\end{Bmatrix}A\begin{Bmatrix}l'_x & \sigma'_x & j'_x\\ l'_y & s_4 & j'_y\\ l'_{xy} & \sigma' & J'_3\end{Bmatrix}A\begin{Bmatrix}l_{xy} & \sigma & J_3\\ l_z & s_4 & j_z\\ L & S & J\end{Bmatrix}A\begin{Bmatrix}l'_{xy} & \sigma' & J'_3\\ l'_z & s_2 & j'_z\\ L & S & J\end{Bmatrix}$$

$$\times A\begin{Bmatrix}l'_x & l'_y & l'_{xy}\\ l'_z & L & l'_{yz}\end{Bmatrix}A\begin{Bmatrix}l'_x & \lambda & l_{xy}\\ l_z & L & l'_{yz}\end{Bmatrix}(-)^{s_1+s_2-\sigma_x+s_2+\sigma'-S}A\begin{Bmatrix}s_2 & s_1 & \sigma_x\\ s_3 & \sigma & \sigma'_x\end{Bmatrix}$$

$$\times A\begin{Bmatrix}s_2 & \sigma'_x & \sigma\\ s_4 & S & \sigma'\end{Bmatrix}\frac{xyz}{x^g_{\alpha\alpha'}y^g_{\alpha\alpha'}z^g_{\alpha\alpha'}}\mathcal{H}^{l_{xy}}_{l_xl_y,l'_x\lambda}(x,y,u)\mathcal{H}^{l'_{yz}}_{\lambda l_z,l'_yl'_z}(y_0,z,v)$$

with the constraints $\cos(\widehat{\hat{x},\hat{y}})=u$ and $\cos(\widehat{\hat{y}_0,\hat{z}})=v$, and where

$$t_{\alpha,\alpha'}=(-)^{t_1+t_2-\tau_x+t_2+T'_3-T}A\begin{Bmatrix}t_2 & \tau'_x & T_3\\ t_4 & T & T'_3\end{Bmatrix}A\begin{Bmatrix}t_2 & t_1 & \tau_x\\ t_3 & T_3 & \tau'_x\end{Bmatrix}.$$

b. α' of H type

We define again $x^g_{\alpha\alpha'},y^g_{\alpha\alpha'},z^g_{\alpha\alpha'}$ and an intermediate coordinate $\vec{y}_0$ in the following way:

$$\begin{pmatrix}\vec{x}^g_{\alpha\alpha'}\\ \vec{y}^g_{\alpha\alpha'}\\ \vec{z}^g_{\alpha\alpha'}\end{pmatrix}=\begin{pmatrix}1 & 0 & 0\\ 0 & -\frac{1}{\sqrt{3}} & \frac{\sqrt{2}}{\sqrt{3}}\\ 0 & \frac{\sqrt{2}}{\sqrt{3}} & \frac{1}{\sqrt{3}}\end{pmatrix}\begin{pmatrix}\vec{x}^g_{\alpha\alpha'}\\ \vec{y}_0\\ \vec{z}\end{pmatrix}\quad\text{and}\quad\begin{pmatrix}\vec{x}^g_{\alpha\alpha'}\\ \vec{y}_0\\ \vec{z}\end{pmatrix}=\begin{pmatrix}\frac{1}{2} & \frac{\sqrt{3}}{2} & 0\\ \frac{\sqrt{3}}{2} & -\frac{1}{2} & 0\\ 0 & 0 & 1\end{pmatrix}\begin{pmatrix}\vec{x}\\ \vec{y}\\ \vec{z}\end{pmatrix}.$$

The corresponding expression for $g_{\alpha\alpha'}$ is now

$$g_{\alpha,\alpha'}(x,y,z,u,v)=\frac{\varepsilon}{2}t_{\alpha,\alpha'}\sum_{l_{xy},\sigma,l'_{xy},l'_{yz},L,S,\lambda}A\begin{Bmatrix} l_x & \sigma_x & j_x \\ l_y & s_3 & j_y \\ l_{xy} & \sigma & J_3 \end{Bmatrix}A\begin{Bmatrix} l'_x & \sigma'_x & j'_x \\ l'_y & \sigma'_y & j'_y \\ l'_{xy} & S & j'_{xy} \end{Bmatrix}A\begin{Bmatrix} l_{xy} & \sigma & J_3 \\ l_z & s_4 & j_z \\ L & S & J \end{Bmatrix}$$

$$\times(-)^{l'_{xy}+S-J'_3+L+S-J}A\begin{Bmatrix} S & l'_{xy} & J'_3 \\ l'_z & J & L \end{Bmatrix}A\begin{Bmatrix} l'_x & l'_y & l'_{xy} \\ l'_z & L & l'_{yz} \end{Bmatrix}A\begin{Bmatrix} l'_x & \lambda & l_{xy} \\ l_z & L & l'_{yz} \end{Bmatrix}$$

$$\times(-)^{s_1+s_3-\sigma'_x+\sigma_x+s_3-\sigma}A\begin{Bmatrix} \sigma'_x & s_2 & \sigma \\ s_4 & S & \sigma'_y \end{Bmatrix}A\begin{Bmatrix} s_3 & s_1 & \sigma'_x \\ s_2 & \sigma & \sigma_x \end{Bmatrix}\frac{xyz}{x^g_{\alpha\alpha'}y^g_{\alpha\alpha'}z^g_{\alpha\alpha'}}\mathcal{H}^{l_{xy}}_{l_xl_y,l'_x\lambda}(x,y,u)\mathcal{H}^{l'_{yz}}_{\lambda l_z,l'_yl'_z}(y_0,z,v),$$

where $t_{\alpha,\alpha'}=(-)^{t_1+t_3-\tau'_x+\tau_x+t_3-T_3}A\{^{\tau'_x t_2 T_3}_{t_4 T \tau'_y}\}A\{^{t_3 t_1 \tau'_x}_{t_2 \tau_y \tau_x}\}$ and with the constraints $\cos(\widehat{\hat{x},\hat{y}})=u$ and $\cos(\widehat{\hat{y}_0,\hat{z}})=v$.

[1] N. W. Schellingerhout, J. J. Schut, and L. P. Kok, Phys. Rev. C **46**, 1192 (1992).
[2] W. Glöckle and H. Kamada, Phys. Rev. Lett. **71**, 971 (1993).
[3] W. Glöckle, H. Witala, D. Hüber, H. Kamada, and J. Golak, Contribution to the *International Conference on Few-Body Problems in Physics*, Williamsburg, Virginia 1994, AIP Conf. Proc. No. 334, edited by F. Gross (AIP, New York, 1995).
[4] M. Viviani, A. Kievsky, and S. Rosati, Few-Body Syst. **18**, 25 (1995).
[5] J. A. Tjon, Phys. Lett. **63B**, 391 (1976).
[6] A. C. Fonseca, Phys. Rev. C **30**, 35 (1984).
[7] A. C. Fonseca, Phys. Rev. C **40**, 1390 (1989).
[8] A. C. Fonseca, Few-Body Syst., Suppl. **7**, 177 (1994).
[9] E. Uzu, S. Oryu, and M. Tanifuji, Prog. Theor. Phys. **90**, 937 (1993).
[10] E. Uzu, S. Oryu, and M. Tanifuji, Few-Body Syst., Suppl. **8**, 97 (1995).
[11] A. Arriaga, V. R. Pandharipande, and R. Schiavilla, Phys. Rev. C **43**, 983 (1991).
[12] R. Schiavilla, J. Carlson, and R. B. Wiringa, Contribution to the *International Conference on Few-Body Problems in Physics* [3], p. 79.
[13] S. L. Yakovlev and I. N. Filikhin, Phys. At. Nucl. **58**, 754 (1995).
[14] H. M. Hofmann and G. M. Hale, Nucl. Phys. **A613**, 69 (1997).
[15] J. Carbonell, C. Gignoux, and S. P. Merkuriev, Few-Body Syst. **15**, 15 (1993).
[16] F. Ciesielski, J. Carbonell, and C. Gignoux, Nucl. Phys. **A631**, 653c (1998).
[17] O. A. Yakubowsky, Sov. J. Nucl. Phys. **5**, 937 (1967).
[18] L. D. Faddeev, Sov. Phys. JETP **39**, 1459 (1960).
[19] L. D. Faddeev, Sov. Phys. JETP **12**, 1014 (1961).
[20] F. Ciesielski, Ph.D. thèse, Université J. Fourier Grenoble, 1997.
[21] S. P. Merkuriev, S. L. Yakovlev, and C. Gignoux, Nucl. Phys. **A431**, 125 (1984).
[22] J. R. Taylor, *Scattering Theory* (Wiley, New York, 1972).
[23] Gy. Bencze, C. Chandler, A. G. Gibson, and G. W. Pletsch, Few-Body Syst. **18**, 213 (1995).
[24] G. L. Payne, in *Models and methods in few-body physics*, edited by L. S. Ferreira *et al.*, Vol. 273 of Lecture Notes in Physics (Springer, Berlin, 1987), p. 64.
[25] N. W. Schellingerhout, L. P. Kok, and G. D. Bosveld, Phys. Rev. A **40**, 5568 (1989).
[26] N. W. Schellingerhout and L. P. Kok, Nucl. Phys. **A508**, 290 (1990).
[27] N. W. Schellingerhout, Ph.D thesis, Groningen University, 1995.
[28] Y. Saad and M. H. Schultz, SIAM (Soc. Ind. Appl. Math.) J. Sci. Stat. Comput. **7**, 856 (1986).
[29] N. W. Schellingerhout, L. P. Kok, and G. D. Bosveld, Phys. Rev. A **40**, 5568 (1989).
[30] R. A. Malfliet and J. A. Tjon, Nucl. Phys. **A127**, 161 (1969).
[31] Y. Saad, *Numerical Methods for Large Eigenvalue Problems*, Manchester University Press Series in Algorithms and Architectures for Advanced Scientific Computing (Manchester University Press, New York, 1992).
[32] R. A. Aziz and M. J. Slaman, J. Chem. Phys. **94**, 8047 (1991).
[33] G. L. Payne, J. L. Friar, and B. F. Gibson, Phys. Rev. C **26**, 1385 (1982).
[34] H. Kamada and W. Glöckle, Nucl. Phys. **A548**, 205 (1992).
[35] D. R. Tilley, H. R. Weller, and G. M. Hale, Nucl. Phys. **A541**, 1 (1992).
[36] J. Blomqvist, Nucl. Phys. **A103**, 644 (1967).
[37] S. K. M. Wong, G. Saunier, and B. Rouben, Nucl. Phys. **A169**, 294 (1971).
[38] R. Ceuleneer, P. Vandepeutte, and C. Semay, Phys. Rev. C **38**, 2335 (1988).
[39] S. K. Adhikari, Phys. Rev. C **24**, 16 (1981).
[40] T. W. Phillips, B. L. Berman, and J. D. Seagrave, Phys. Rev. C **22**, 384 (1980).
[41] J. D. Seagrave, B. L. Berman, and T. W. Phillips, Phys. Lett. B **91**, 200 (1980).
[42] A. Laverne and C. Gignoux, Rapport Interne Report No. ISN72.11.
[43] H. Rauch, D. Tuppinger, H. Wölwitsch, and T. Wroblewski, Phys. Lett. B **165**, 39 (1985).
[44] G. M. Hale, D. C. Dodder, J. D. Seagrave, B. L. Berman, and T. W. Phillips, Phys. Rev. C **42**, 438 (1990).